Cancer Immunol Immunother (2010) 59:355–366
DOI 10.1007/s00262-009-0754-z

ORIGINAL ARTICLE

A humanized anti-osteopontin antibody inhibits breast cancer growth and metastasis in vivo

Jianxin Dai · Bohua Li · Jinping Shi · Ling Peng · Dapeng Zhang · Weizhu Qian · Sheng Hou · Lei Zhao · Jie Gao · Zhiguo Cao · Jian Zhao · Hao Wang · Yajun Guo

Received: 7 December 2008 / Accepted: 3 August 2009 / Published online: 19 August 2009

Abstract Osteopontin (OPN) has been implicated as an important mediator of breast cancer progression and metastasis and has been investigated for use as a potential therapeutic target in the treatment of breast cancer. However, the in vivo antitumor effect of anti-OPN antibodies on breast cancer has not been reported. In this study, a mouse anti-human OPN antibody (1A12) was humanized by complementarity-determining region grafting method based on computer-assisted molecular modeling. A humanized version of 1A12, denoted as hu1A12, was shown to possess affinity comparable to that of its parental antibody. The ability of hu1A12 to inhibit cell migration, adhesion, invasion and colony formation was assessed in a highly metastatic human breast cancer cell line MDA-MB-435S. The results indicated that hu1A12 was effective in inhibiting the cell adhesion, migration, invasion and colony formation of MDA-MB-435S cells in vitro. hu1A12 also showed significant efficacy in suppressing primary tumor growth and spontaneous metastasis in a mouse lung metastasis model of human breast cancer. The specific epitope recognized by hu1A12 was identified to be ^{212}NAPSD^{216}, adjacent to the calcium binding domain of OPN. Our data strongly support that OPN is a potential target for the antibody-based therapies of breast cancer. The humanized anti-OPN antibody hu1A12 may be a promising therapeutic agent for the treatment of human breast cancer.

Keywords Breast cancer · Humanized antibody · Immunogenicity · Metastasis · Osteopontin

Introduction

Osteopontin (OPN) is a secreted glycophosphoprotein that has been implicated in both physiologic and pathologic processes [1]. Cell types which express OPN include osteoclasts, osteoblasts, epithelial cells of the breast, kidney, skin, nerve cells, vascular smooth muscle cells, endothelial cells and activated immune cells [2, 3]. A high level of OPN expression is one of the features often associated with highly metastatic cancer cells [4–6]. The metastatic activity of various cancer cells can be significantly inhibited by downregulating OPN expression [7–10]. For example, silencing of OPN expression by siRNA suppressed CT26 murine colon adenocarcinoma metastasis both in vitro and in vivo [11]. On the other hand, an increase in OPN expression levels has been shown to correlate with the enhanced malignancy [2, 12, 13].

Breast cancer is one of the leading causes of death from cancer among women. The majority of these breast cancer deaths are due to the propensity of primary breast tumors to metastasize to regional and distant sites such as lymph node, lung, liver, brain and bone [13, 14]. Current surgical and medical treatments have only limited success in reducing the breast cancer recurrence rate [15, 16]. Thus, there is an urgent need to develop new therapeutics for the

J. Dai, B. Li and J. Shi contributed equally to this work as first authors.

J. Dai · B. Li · J. Shi · L. Peng · D. Zhang · W. Qian · S. Hou · L. Zhao · J. Gao · Z. Cao · J. Zhao · H. Wang · Y. Guo (✉)
International Joint Cancer Institute and 301 General Hospital Cancer Center, The Second Military Medical University, 800 Xiang Yin Road, 200433 Shanghai, People's Republic of China
e-mail: yjguo@smmu.edu.cn

B. Li · D. Zhang · W. Qian · S. Hou · H. Wang · Y. Guo
National Engineering Research Center for Antibody Medicine, 399 Libing Road, 201203 Shanghai, People's Republic of China

treatment of breast cancer. Previous studies have indicated that OPN levels are elevated in the blood and primary tumors of breast cancer patients, and in some cases this has been correlated with poor prognosis [17–20]. The highly metastatic human breast cancer cell line expresses significantly higher levels of OPN than does the low metastatic one [21]. OPN knockdown by shRNA suppresses tumorigenicity of human metastatic breast carcinoma MDA-MB-435 [22]. Silencing of OPN by its specific siRNA was demonstrated to effectively attenuate breast cancer progression in mice [7]. Previous studies also indicated that downregulation of OPN by OPN-specific shRNA effectively inhibited the metastasis of human metastatic breast cancer cell line in severe combined immunodeficient mice [23].

Owing to its role in stimulating breast cancer growth and metastasis, OPN may become a candidate target for the antibody-based therapies of human breast cancer. A mouse anti-human OPN antibody has been demonstrated to be able to inhibit the adhesion of human breast cancer cells [24]. However, the in vivo antitumor effect of anti-OPN antibodies on breast cancer has not yet been reported. In this study, a humanized anti-OPN antibody was generated by complementarity-determining region (CDR) grafting method based on computer-assisted molecular modeling, and its antitumor activity in vitro and in vivo was investigated on a highly metastatic human breast cancer cell line, MDA-MB-435S. The humanized antibody was shown to be able to effectively inhibit the cell adhesion, migration, invasion and colony formation of MDA-MB-435S cells. Therapeutic studies further demonstrated that this humanized anti-OPN antibody was effective in suppressing primary tumor growth and spontaneous metastasis in a mouse lung metastasis model of human breast cancer, suggesting that it might be a promising therapeutic agent for the treatment of human breast cancer.

Materials and methods

Materials

MDA-MB-435S cell line, which expresses high levels of OPN and is known to be tumorigenic and highly metastatic, was obtained from the American Type Culture Collection (ATCC). The recombinant human OPN protein was expressed in yeast cells and purified. The 1A12 hybridoma cell line secreting mouse monoclonal antibody (mAb) against human OPN was generated by the standard hybridoma technique in our laboratory. The mouse mAb 1A12 (IgG1, κ) was purified by Protein A affinity chromatograph from 1A12 hybridoma cell culture supernatant. Peptides used in this study were synthesized by Yeli Bio-Scientific Inc. (Shanghai, China). Six-week-old female BALB/c mice and athymic nude mice were obtained from Shanghai Experimental Animal Center of Chinese Academy of Sciences. All animals in this study were housed under pathogen-free conditions and were treated in accordance with guideline of the Committee on Animals of the Second Military Medical University.

Cloning of anti-OPN mAb heavy and light chain variable region genes

Total RNA was isolated from 1A12 hybridoma cells with TRIzol Reagent (Invitrogen, Carlsbad, CA). The heavy and light variable region cDNAs of 1A12 mAb were cloned using 5'RACE system (Invitrogen, Carlsbad, CA) by the method described previously [25]. The final PCR products were cloned into pGEM-T vector (Promega, Madison, WI) for sequence determination.

Molecular modeling of variable fragment (Fv) of the 1A12 mAb

The Protein Data Bank (PDB) was searched for antibody sequences that had high sequence identity with the 1A12 Fv. Two separate BLASTP searches were performed for light chain variable region (V_L) and heavy chain variable region (V_H) of 1A12. To construct the three-dimensional structure of the 1A12 Fv by homology modeling (INSIGHT II 2003, Accelrys, San Diego, CA), the sequences of V_L and V_H of 1A12 and their templates were aligned, respectively. The coordinates for the structurally conserved regions were assigned from the template and the loop regions were generated by Homology program. The newly built structure was subjected to molecular dynamics simulations and then energy minimized by 1,000 steps of the steepest descent method and followed by conjugate gradient method using Discover program. Finally, the refined model was assessed by Profile-3D program.

Humanization of anti-OPN mAb 1A12

V_L and V_H of 1A12 were subjected separately to a BLASTP search against the entire non-redundant Genbank database (PDB, SwissProt, SPupdate, PIR). Human antibody variable regions that were the most homologous in sequence to 1A12 variable regions were chosen as the human framework (FR) for the humanized version of 1A12. The CDRs in the humanized antibody were chosen to be identical to those in the murine antibody 1A12. The transfer of CDRs alone often results in a significant loss of antigen binding because certain murine FR residues are critical for preserving the CDR conformations or are directly involved in antigen binding. Therefore, these key FR residues of mouse antibodies must be substituted into the human

acceptor framework to restore affinity [26–28]. The molecular model of the 1A12 Fv showed that some FR residues were close enough to the CDRs to either influence their conformations or interact directly with antigen. When these FR residues differed between 1A12 and the human antibody template, the residue in the humanized antibody was chosen to be the murine 1A12 residue rather than the human antibody residue. The light and heavy chain variable region genes of humanized versions of 1A12 were synthesized by overlapping PCR method.

Construction and expression of recombinant antibodies

The light and heavy chain expression vectors for chimeric and humanized antibodies were constructed using the same method as described previously [25]. Appropriate light and heavy expression vectors for recombinant antibodies were co-transfected into COS-7 cells using Lipofectamine 2000 reagent (Invitrogen, San Diego, CA) according to the manufacturer's instruction. After 48 h incubation, the supernatants were collected and analyzed by enzyme-linked immunosorbent assay (ELISA) for quantitation of antibodies. The ELISA assay used goat anti-human IgG Fc (KPL, Gaithersburg, MD) as capture antibody and goat anti-human kappa horseradish peroxidase (HRP) (Southern Biotechnology Associates, Birmingham, AL) as detecting antibody.

OPN binding assays

For measuring the OPN binding activity of anti-OPN chimeric and humanized antibodies, ELISA plates were coated with human OPN. After washing and blockade of free protein-binding sites, different concentrations of recombinant mAbs were added to each well and incubated for 1 h. After washing, HRP-conjugated goat anti-mouse IgG (KPL) was added and the plates were further incubated for 1 h. Finally, 3,3′,5,5′-tetramethylbenzidine (TMB) was added as a substrate and the absorbance was measured at 450 nm.

Stable expression and purification of recombinant antibodies

Appropriate light and heavy expression vectors were co-transfected into Chinese hamster ovary (CHO)-K1 cells using Lipofectamine 2000 reagent. Stable transfectants were isolated using the same method as described previously [25]. The clones producing the highest amount of recombinant antibodies were selected and grown in serum-free medium. Finally, recombinant antibodies were purified by Protein A affinity chromatography from the serum-free culture supernatant.

Biacore analysis

The kinetic parameters of anti-OPN antibodies for OPN were determined using the Biacore T100 instrument (Biacore AB, Uppsala, Sweden) according to the manufacturer's instructions. Briefly, covalent immobilization of purified recombinant human OPN onto a Series S CM5 sensor chip (Biacore) was performed using an amine coupling kit (Biacore). Twofold serial dilutions of anti-OPN antibodies were injected over the sensor chip surface at a flow rate of 50 μl/min. Irrelevant antibodies were used as controls. The association (K_a) and dissociation (K_d) rate constants of anti-OPN antibodies were determined using the Biacore T100 Evaluation software version 2.0 (Biacore).

Scratch-wound healing assay

MDA-MB-435S cells were cultured to subconfluence in 12-well plates. Streaks were made on the monolayer culture with 10 μl pipette tips. After washing away suspended cells, the cells were refed with medium containing OPN in the presence or absence of the humanized anti-OPN antibody (25 μg/ml). The progress of migration was photographed immediately or 18 h after wounding.

Cell adhesion assay

The 96-well microtitre plates were coated with OPN (10 μg/ml), followed by treatment with 1% BSA for 1 h at 37°C. 5×10^4 MDA-MB-435S cells were added to each well in the presence or absence of the humanized anti-OPN antibody (25 μg/ml). After 2 h incubation at 37°C, the medium was removed and washed twice with PBS gently. The adherent cells were fixed in 1% methanol, stained with 0.5% crystal violet and lysed with 2% Triton X-100. The absorbance was measured at 595 nm.

Invasion assay

Cell invasion was measured using a 24-well Transwell system with a polycarbonate filter membrane of 8 μm pore size (Corning, Cambridge, MA). The upper side of the filter was coated with Matrigel (BD Bioscience, Bedford, MA). 5×10^5 MDA-MB-435S cells with or without the humanized anti-OPN antibody (25 μg/ml) were added to the top chamber and 600 μl medium containing OPN (5 μM) was added to the bottom chamber. After 24 h, the non-migrating cells on the upper side of the filter were scraped and washed. The migrating cells on the reverse side of the filter were stained with crystal violet and counted. All assays were performed in triplicate.

Colony formation in soft agar

MDA-MB-435S cells (1×10^4 ml^{-1}) suspended in 0.3% agar solution were plated onto a layer of 0.5% agar solution in 24-well culture plates. Every other day, 0.2 ml per well of medium containing the humanized anti-OPN antibody (25 μg/ml) or control human IgG was added. After 10 days, the colonies containing at least 50 cells were counted. All assays were performed in triplicate.

Proliferation and apoptosis assays

The MDA-MB-435S were seeded at 2×10^4 cells per well in 96-well plates and allowed to adhere overnight before experimentation. The cells were serum-starved, and OPN (5 μM) with or without anti-OPN antibodies (20 μg/ml) was added and incubated for 24 h. For proliferation assay, 1 μCi per well [3H]thymidine was added and incubated for an additional 6 h at 37°C. Cells were washed, fixed with 10% trichloroacetic acid, and counted. For apoptosis assay, the apoptosis of MDA-MB-435S was determined by nuclear fragmentation of 4′-6-diamidino-2-phenylindole (DAPI)-stained cells. All assays were performed in triplicates and repeated three times.

Western blot analysis

Total protein was isolated from MDA-MB-435S receiving different treatments. SDS-PAGE (12%) gels were run and subsequently transferred to nitrocellulose membranes. The membranes were then blocked in 10% milk in PBS overnight at 4°C. Primary antibodies (Bcl-2, Bax, and β-actin) were added for 1 h at room temperature followed by the addition of appropriate HRP-conjugated secondary antibody. Membranes were exposed to chemiluminescence reagents for 1 min, and bands were detected by exposing to an X-ray film.

Electrophoretic mobility shift assay (EMSA)

The DNA activity of nuclear factor κB (NF-κB) was determined by EMSA. A double-stranded oligonucleotide containing the DNA-binding site for the NF-κB proteins (forward, 5′-AGTTGAGGGGACTTTCCCAGGC-3′; reverse, 5′-GC CTGGGAAAGTCCCCTCAACT-3′) was end-labeled using biotin. The MD-MB-435S cells were treated with OPN (5 μM) with or without anti-OPN antibodies (20 μg/ml) for 6 h. Nuclear proteins were extracted with NE-PER nuclear and cytoplasmic extraction reagents (Pierce, Rockford, IL). The nuclear extracts (3 μg) were incubated with 20 fmol of biotin-labeled double-stranded NF-κB oligonucleotide in binding buffer. The DNA-binding complex was resolved on a native polyacrylamide gel and was analyzed.

Animal study

Groups of 20 female nude mice were anesthetized and a small incision (0.5 mm) was made in the skin over the right lateral thorax. The mammary fat pads (mfps) were exposed and 5×10^6 MDA-MB-435S cells were orthotopically injected into the mfps at day 0. Then the mice were injected i.p. with the humanized 1A12 antibody or control human IgG (5 mg/kg body weight) twice per week for 4 weeks. For each group, ten animals were used to determine primary tumor growth rate and killed at day 70; the other ten were killed at day 50 and lungs, brain, heart, bone, liver and lymph nodes were collected to examine spontaneous remote metastases. Tumor volume was estimated using the formula: tumor volume (mm^3) = length × $(\text{width})^2/2$.

Lung tissue sections were analyzed by H&E staining and lung metastatic foci were counted as described previously [29]. Briefly, a total of 100 serial sections were made for every half of the lung tissue blocks, and the first of every decade of sections were analyzed under the microscope for the presence of the tumor cell clusters by two pathologists. The grades of metastatic foci were defined as follows: grade I, <20 cells/foci; grade II, 20 < cells < 50/foci; grade III, 50 < cells < 100 cells/foci, grade IV, >100 cells/foci.

Epitope mapping of the humanized 1A12 antibody

The Ph.D.-12 Phage Display Peptide Library (New England Biolabs, Beverly, MA) were used for biopanning. Biopanning was performed as described in our previous report [30]. After three rounds of panning, positive phage clones were subjected to DNA sequence analysis.

Immunochemical assay

The reactivity of the humanized 1A12 antibody with synthetic peptides was determined by ELISA assay. Briefly, 96-well plates were coated with KLH peptide. Following washing and blockade of free protein-binding sites, different concentrations of the humanized 1A12 antibody were added to each well. After 4 h incubation, the antibody binding to peptide was detected by sequential addition of an appropriate dilution of HRP-conjugated goat anti-human IgG (Zymed, San Francisco, CA). After the addition of TMB and stop solution, absorbance was read at 450 nm by an immunoreader.

The ability of synthetic peptides to block the interaction between the humanized 1A12 antibody and OPN was also investigated. Briefly, mAb was incubated with different concentrations of synthetic peptides for an hour. Then the mixture was respectively added to 96-well plates precoated with OPN. After 2 h incubation, the wells were washed and the antibody binding to OPN was detected with an appropriate dilution of HRP-conjugated goat anti-human

IgG. After the addition of TMB and stop solution, absorbance was read at 450 nm by an immunoreader.

Statistical analysis

Statistical analysis was performed by Student's unpaired *t* test to identify significant differences unless otherwise indicated. Differences were considered significant at a P value of <0.05.

Results

Molecular modeling of 1A12 Fv

The nucleotide sequences of V_H and V_L of 1A12 were determined and deposited in GenBank under the accession numbers EU926488 and EU926489, respectively. The deduced amino acid sequences of V_H and V_L were shown in Fig. 1. We searched PDB for antibody sequences with high sequence identity with the 1A12 antibody variable regions. The V_L and V_H of the murine monoclonal antibody mAb735 (PDB no. 1PLG) specific for α-(2→8)-linked polysialic acid, respectively, show 92 and 72% identity with the V_L and V_H of 1A12. The crystallographic resolution of murine monoclonal antibody mAb735 is 2.8 Å and we selected it as the template of 1A12. Then the molecular model of the 1A12 Fv was obtained by Insight II molecular modeling software (Fig. 2).

Humanization of 1A12 mAb

The V_H and V_L of 1A12 were respectively subjected to BLASTP searches against the entire non-redundant Genbank database. The V_H of the human antibody CAA79298 (GenBank no. CAA79298) was 67% identical to the 1A12 heavy chain variable region and the V_L of human antibody BAC01734 (GenBank no. BAC01734) was 81% identical to the 1A12 light chain variable region. We selected the variable regions of these two human antibodies as frameworks for the V_H and V_L of humanized 1A12 antibody,

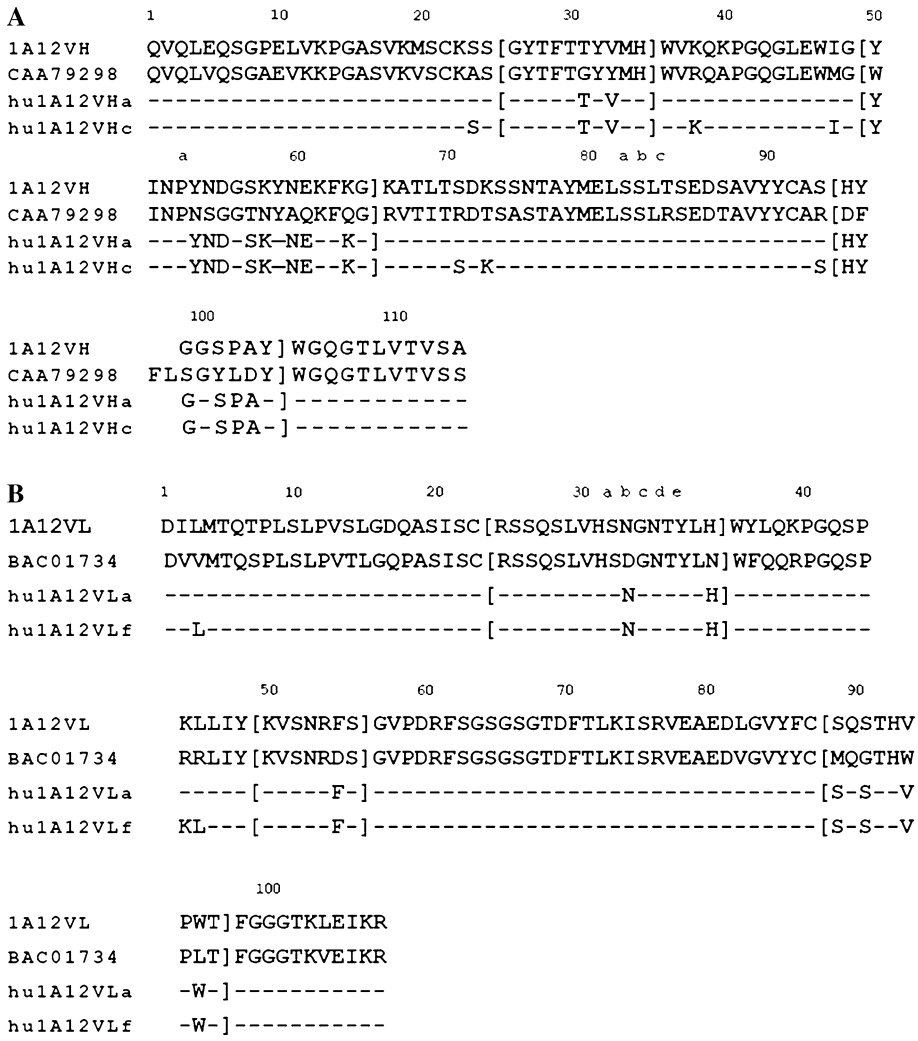

Fig. 1 Amino acid sequences of humanized 1A12 antibody heavy (**a**) and light (**b**) chain variable regions. 1A12VH and 1A12VL indicate heavy and light chain variable regions of murine 1A12 monoclonal antibody, respectively. The heavy chain variable region of human antibody CAA79298 was chosen as framework for the humanized heavy chain and the light chain variable region of human antibody BAC01734 was chosen for the humanized light chain. hu1A12VHa and hu1A12VHc indicate different versions of humanized heavy chain variable regions. hu1A12VLa and hu1A12VLf indicate different versions of humanized light chain variable regions. The *dashes* represent amino acids that are the same as the corresponding residues in human antibodies CAA79298 or BAC01734. The CDRs are enclosed with *brackets*. Amino acids (in *one-letter notation*) are numbered according to Kabat et al. [31]

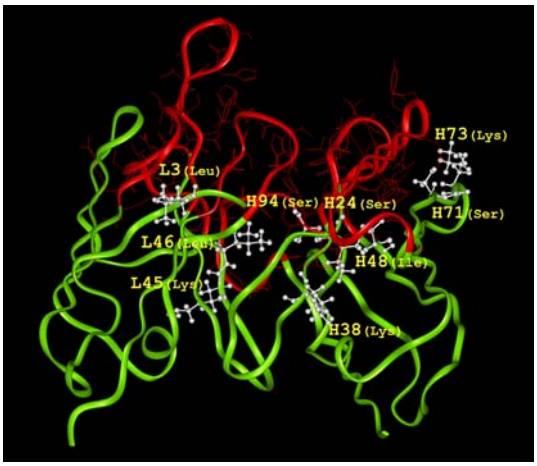

Fig. 2 Molecular model of the 1A12 variable regions. The 1A12 variable regions are shown by a *solid ribbon* representation. The FRs are shown in *light gray* (*green* in color picture) and the CDRs are shown in *dark gray* (*red* in color picture). Nine FR residues, L3, L45, L46, H24, H38, H48, H71, H73 and H94, which are within about 5 Å of the CDRs and are of potential importance to the antigen binding, are shown in *white*

respectively. First, the three CDRs from 1A12 light chain or heavy chain were directly grafted into human antibody light chain or heavy chain frameworks to generate humanized antibody genes. The humanized V_L and V_H were cloned into expression vectors, respectively, and were coexpressed in COS-7 cells, yielding humanized version (hu1A12Ha/hu1A12La). The amino acid sequence of the humanized antibody was shown in Fig. 1. Our results indicated that this humanized antibody lost its binding activity (Fig. 3a), suggesting that some FR residues in this humanized version must be back-mutated to reconstitute the full binding activity. With the help of graphic manipulation, nine mouse FR residues, which differed between 1A12 and the human antibody template, were observed to be within 5 Å of the CDRs and to probably affect the structure of the CDRs (Fig. 2). A number of humanized light and heavy chain versions were constructed to evaluate the contribution of each of the nine FR residues to antigen binding. Finally, a humanized version (hu1A12Hc/hu1A12Lf) showing the similar antigen-binding activity as the chimeric 1A12 antibody (c1A12) was obtained (Fig. 3a). This humanized antibody was designated as hu1A12 and its amino acid sequences were shown in Fig. 1.

Measurement of kinetic binding constants of anti-OPN antibodies

Kinetic binding constants of c1A12 and hu1A12 for OPN were determined using Biacore T100 instrument. Results of the kinetic analysis were shown in Fig. 3b and c. Although the on-rate (K_a) of hu1A12 was slightly slower than that of c1A12, the off-rate (K_d) of hu1A12 was also slower. Thus, hu1A12 was shown to possess similar affinity (KD) as its chimeric counterpart (Fig. 3c).

hu1A12 inhibits MDA-MB-435S cell migration, adhesion, invasion and colony formation

To investigate the in vitro antitumor activity of the humanized anti-OPN antibody hu1A12, we performed cell migration, adhesion, invasion and colony formation assays. The ability of hu1A12 to suppress MDA-MB-435S cell migration was evaluated by scratch-wound healing assays. The results shown in Fig. 4a indicated that hu1A12 significantly inhibited breast cancer cell motility compared with the control human IgG. The cell adhesion assay results also demonstrated that hu1A12 was effective in inhibiting the cell adhesion of MDA-MB-435S cells to human OPN (Fig. 4b).

Matrigel invasion assay was performed to study the effect of hu1A12 on the invasion ability of MDA-MB-435S cells. As shown in Fig. 4c, hu1A12 significantly inhibited cell invasion through Matrigel-coated filters as compared to the control human IgG. We next examined the efficacy of hu1A12 in inhibiting the tumor cell anchorage-independent growth (soft agar colony formation). The anchorage-independent growth ability of cancer cells correlates closely with their in vivo tumorigenicity. The results shown in Fig. 4d demonstrated that hu1A12-treated MDA-MB-435S cells formed significantly less colonies in soft agar than control human IgG-treated cells, suggesting that hu1A12 could effectively suppress the anchorage-independent growth ability of breast cancer cells.

Hu1A12 inhibits OPN-mediated anti-apoptotic and prosurvival functions

We investigated the effect of OPN on proliferation and apoptosis of MDA-MB-435S. The results showed that the addition of OPN to the serum-deprived MDA-MB-435S cells reduced the amount of cell death. In the presence of OPN, [3H]thymidine uptake increased 3.08 ± 0.64-fold in MDA-MB-435S cells (Fig. 5a). However, this incorporation uptake decreased 2.76 ± 0.35-fold when hu1A12 was added. Our results showed that OPN may support cell survival under conditions of serum withdrawal. In the presence of hu1A12, the prosurvival function of OPN was inhibited significantly. Induction of apoptosis was analyzed with the help of DAPI, which caused a regular staining in intact nuclei, but an irregular staining in apoptotic cells. As shown in Fig. 5b, ~30% of MDA-MB-435S lost membrane integrity after treatment with serum deprivation for 24 h, compared with ~10% of cells in control cultures treated with the normal serum culture condition. The MDA-MB-435S treated with OPN showed less DAPI-stained cells compared with non-treated ones.

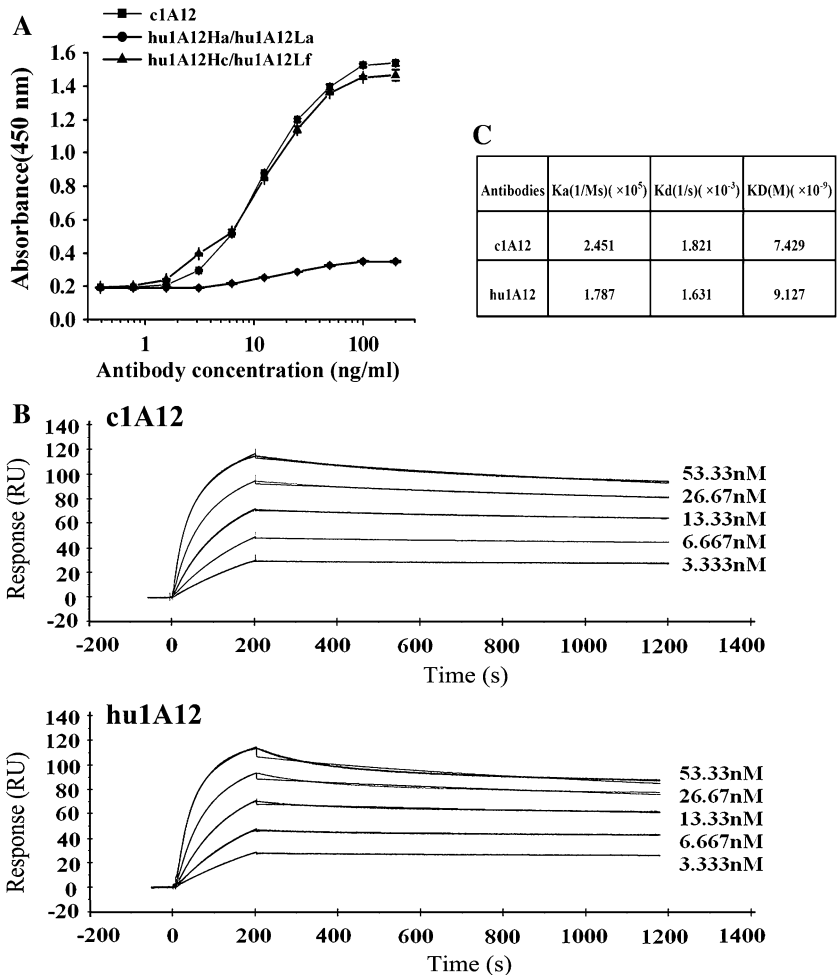

Fig. 3 OPN-binding activity of humanized anti-OPN antibodies (**a**) ELISA assays. Serial log dilutions of c1A12, the humanized version (hu1A12VHa/hu1A12VLa) or the humanized version (hu1A12VHc/hu1A12VLf) were added to ELISA plates pre-coated with human OPN and incubated for 1 h. After washing, mAbs binding to OPN were detected with HRP-conjugated goat anti-mouse IgG. *Points* mean ($n = 3$), *bars* SD. **b** Surface plasmon resonance sensorgrams for binding of anti-OPN antibodies to immobilized OPN. Biacore analysis was performed as described in "Materials and methods". *Curves* were fitted to the bivalent analyte model. **c** Kinetic parameters for anti-OPN antibodies

The expressions of apoptosis-related proteins (Bcl-2 and Bax) were analyzed by Western blot analysis. As shown in Fig. 5c, pro-apoptotic Bax expression was upregulated when hu1A12 was added compared with OPN alone. Conversely, anti-apoptotic Bcl-2 expression was downregulated. The nuclear extracts were prepared and used for EMSA using biotin-labeled NF-κB oligonucleotides. The results shown in Fig. 5d indicated that in OPN-treated MDA-MB-435S, the NF-κB pathway was activated, which provided a protective function to the cells. The DNA–protein complex was specific, as unlabeled NF-κB oligomer inhibited the signal, whereas unrelated oligomer had no effect. In contrast, cells pretreated with hu1A12 did not exhibit NF-κB activity, and the control antibody had no effect inhibiting protective function of OPN.

Hu1A12 inhibits MDA-MB-435S tumor growth and spontaneous lung metastasis in nude mice

The in vivo antitumor effect of the humanized anti-OPN antibody hu1A12 was evaluated in a MDA-MB-435S tumor xenograft mouse model. After MDA-MB-435S cells were implanted in the mfps of female nude mice, all of the mice developed primary tumors. However, hu1A12-treated group had a longer latency period, which took about 50 days to reach a mean tumor volume of ~250 mm^3, while PBS- and control human IgG-treated groups only took about 27 days. Overall, primary tumors in hu1A12-treated mice grew at a slow rate relative to those in control human IgG-treated mice, producing significantly smaller tumor volumes from week 3 to week 12 (Fig. 6a).

The efficacy of hu1A12 in inhibiting tumor metastasis was also investigated. As shown in Table 1, 80–90% of mice treated with PBS or control human IgG developed metastases primarily in the lymph nodes and lungs. Metastases were rarely found in other tissues. The hu1A12-treated mice produced significantly fewer metastases compared to mice injected with PBS or the human IgG control. Moreover, the number of lung metastatic foci in mice from different treatment groups was also compared. The results shown in Fig. 6b clearly indicated that the number of metastatic foci was markedly reduced by treatment with hu1A12 in comparison with either the PBS- or human IgG control-treated group.

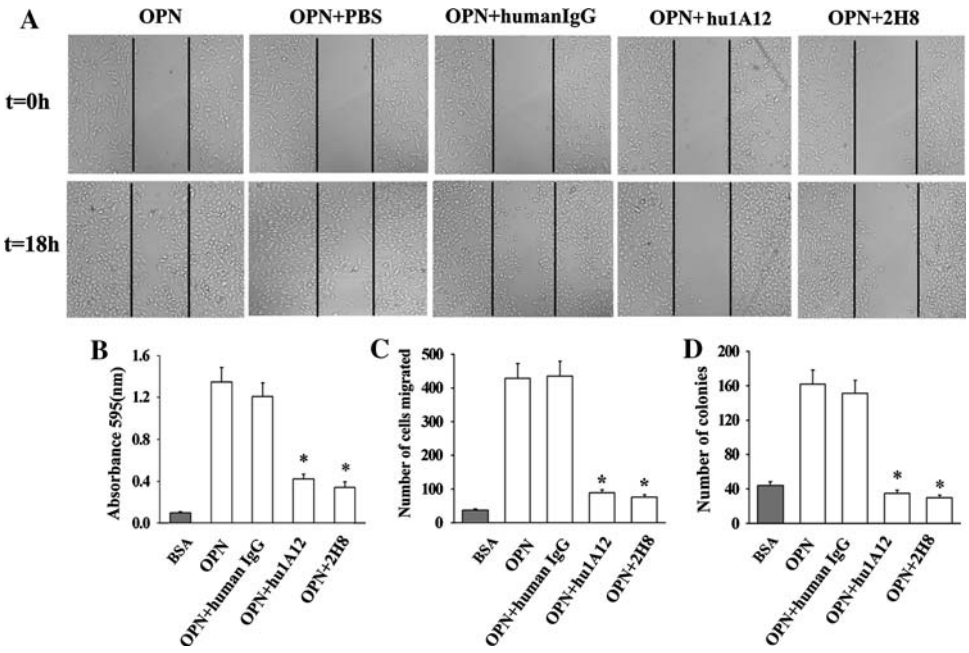

Fig. 4 The inhibition effects of hu1A12 on MDA-MB-435S cell migration, adhesion, invasion and colony formation in soft agar. **a** Cell migration was inhibited by hu1A12. After wounding, MDA-MB-435S monolayer cells were cultured in medium containing OPN in the presence of 25 μg/ml of hu1A12 or control human IgG. Photographs were taken immediately or 18 h after wounding under a Carl Zeiss Axiovert 135 microscope (×40). The data represent one of three experiments with similar results. **b** hu1A12 inhibits cell adhesion to OPN. MDA-MB-435S cells with 25 μg/ml of hu1A12 or control human IgG were added to 96-well plates pre-coated with OPN. After 2 h incubation, unattached cells were washed off and the adherent cells were fixed in 1% methanol, stained with 0.5% crystal violet and lysed with 2% Triton X-100. The absorbance was measured at 595 nm. *Columns* mean ($n = 3$), *bars* SD; $^*P < 0.05$ versus control human IgG. **c** Cell invasion was inhibited by hu1A12. Cell invasion assay was performed using a 24-well Transwell system as described in "Materials and methods". Finally, the cells invading through Matrigel were stained with crystal violet and counted. *Columns* mean ($n = 3$), *bars* SD; $^*P < 0.05$ versus control human IgG. **d** Hu1A12 inhibits the ability of MDA-MB-435S cell to form colonies in soft agar. MDA-MB-435S cells suspended in 0.3% agar solution were plated onto a layer of 0.5% agar solution in 24-well culture plates, followed by the addition of medium containing 25 μg/ml of hu1A12 or control human IgG every other day. Ten days later, the colonies containing at least 50 cells were counted. *Columns* mean ($n = 3$), *bars* SD; $^*P < 0.05$ versus control human IgG. 2H8, a mouse anti-OPN monoclonal antibody specific for RGD domain of OPN, was used as positive control for wound migration, invasion, adhesion, colony formation assays

Mapping of hu1A12-specific epitope on OPN

After the third round of panning, all 35 positive phage clones were sequenced. Alignment of the deduced amino acid sequences of the inserts from these clones resulted in the motif NxNNAPSD and this could be aligned with the ^{212}NAPSD^{216} of OPN (Table 2). The peptide "AQDLNAPSDWDS" containing ^{212}NAPSD^{216} motif in the hOPN was synthesized and denoted as 51P. The ELISA assay results showed that the binding of hu1A12 to 51P-KLH was specific since hu1A12 bound to 51P-KLH but not to control peptide-KLH and 51P-KLH did not react with the irrelevant control mAb (data not shown). To further investigate whether 51P resembled the epitope of hOPN, the capability of 51P to block the binding of hu1A12 to OPN was determined. The results revealed that peptide 51P effectively inhibited the binding of hu1A12 to hOPN. In contrast, irrelevant control peptide did not produce noteworthy inhibition on their interaction (data not shown).

Discussion

The clinical use of murine monoclonal antibodies has been severely limited because repeated doses of foreign immunoglobulin elicit an immune response, referred to as human anti-mouse antibody response (HAMA), which causes rapid clearance of injected antibodies and reduced their efficiency [32, 33]. An early attempt to reduce the immunogenicity is to generate chimeric antibodies which consist of murine antigen binding variable regions fused genetically to human antibody constant regions [34, 35]. To further reduce the immunogenicity of chimeric antibodies, humanized antibodies have been generated by grafting the CDRs of a murine antibody into the corresponding regions of a human antibody [36, 37]. Currently, the humanized antibodies have shown their significant potential as therapeutic agents clinically. In this paper, we have described the humanization of 1A12, a mouse anti-OPN mAb. The initial version of humanized antibody (hu1A12Ha/hu1A12La) was constructed by simply grafting CDRs from 1A12 light

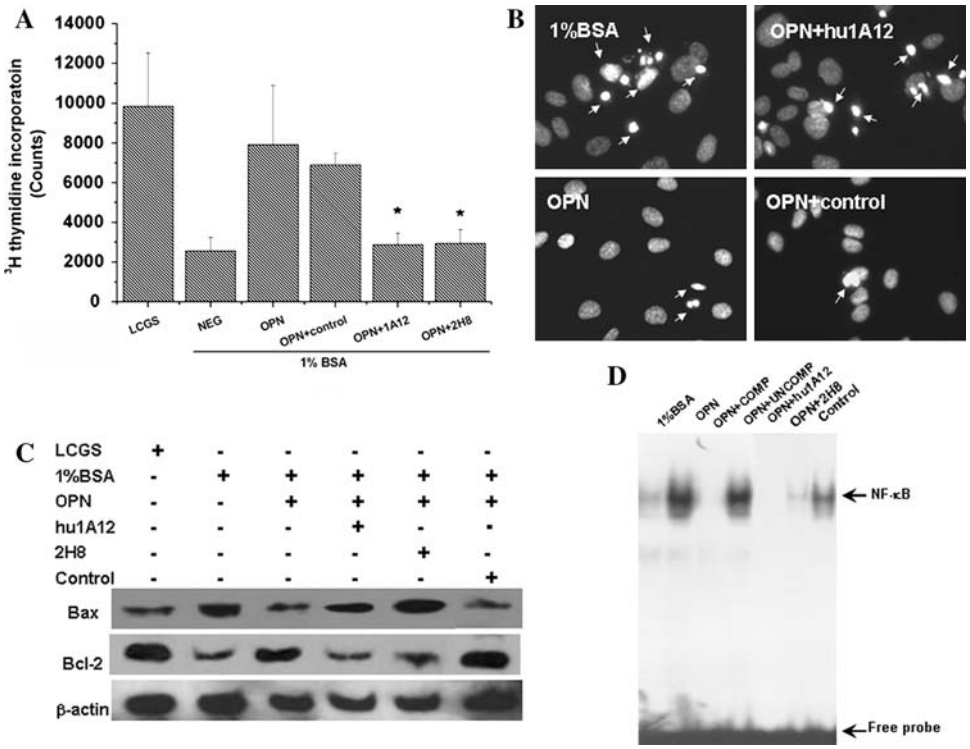

Fig. 5 Effect of anti-OPN antibodies on serum deprivation-induced apoptosis in MDA-MB-435S cells. **a** [^{3}H]thymidine incorporation uptake in MDA-MB-435S. The MDA-MB-435S were maintained in Medium 200 supplemented with low serum growth supplement and were incubated for 24 h. Then the cells were extensively washed with PBS, and the medium was changed to serum-free Medium 200 containing OPN with or without anti-OPN antibodies and incubated for 24 h. Cell proliferation was assayed 24 h after serum deprivation. [^{3}H]thymidine incorporation uptake was examined to present DNA synthesis. Data were expressed as mean ± SD of three experiments, $*P \leq 0.05$. **b** DAPI staining of apoptotic cells. Nuclear morphology was examined by DAPI staining as described in "Materials and methods". Note the nuclear condensation and fragmentation in the serum deprivation group, which was indicative of apoptosis. **c** Bcl-2 family proteins were analyzed by Western blot analysis. The MDA-MB-435S cells were cultured in the presence or absence of OPN (with or without anti-OPN antibodies) for 24 h. After cultivation, we assessed the expression of Bcl-2 and Bax in MDA-MB-435S cells using Western blot analysis. **d** Electrophoretic mobility shift assay was performed to determine the NF-κB activity of OPN- and anti-OPN antibody-treated MDA-MB-435S cells. Compared with untreated MDA-MB-435S, OPN treatment activated NF-κB activity, and anti-OPN antibody treatment abrogated this function. 2H8 is a mouse anti-OPN monoclonal antibody specific for RGD domain of OPN

and heavy chain to human antibody light and heavy chain. The OPN binding activity assay indicated that this humanized version had almost totally lost its antigen-binding activity. It is not surprising, because, in most cases, the transfer of mouse CDR residues alone into human frameworks may alter the structure of the CDRs, resulting in a loss of antigen-binding activity. Consequently, the successful design of humanized antibodies requires that key murine FR residues, which probably affect the structure of the CDRs, are substituted into the human acceptor framework to preserve the CDR conformations [38, 39]. In this study, a reliable three-dimensional model of the variable regions of 1A12 has been built using computer-aided homology modeling. Nine framework amino acids within about 5 Å of the CDRs were identified as key FR residues, which intimately interacted with CDR residues and might affect the structure of the antigen-binding site. Then, a humanized version of 1A12 (hu1A12) was generated by transferring these mouse key framework residues onto the human antibody template that was selected based on homology to 1A12 together with the mouse CDR residues. Biacore assays showed that the affinity equilibrium constant of hu1A12 was similar to that of c1A12, suggesting that this humanized antibody possessed antigen-binding affinity comparable to that of its parental counterpart.

Clinical studies have demonstrated that OPN correlates with disease outcome and survival in patients with metastatic breast cancer and in patients with lymph node-negative breast cancer [17, 18, 40]. OPN has been shown to affecting the behavior of breast cancer cells in a number of ways. Previous studies support the idea that OPN can contribute to the malignancy of breast cancer by influencing pathways involved in the control of cell adhesion, migration, and invasion [41–43]. In the present study, the humanized anti-OPN antibody hu1A12 was demonstrated to be effective in inhibiting the cell adhesion, migration, invasion and colony formation of a highly metastatic human breast cancer cell line, MDA-MB-435S. Previous studies have

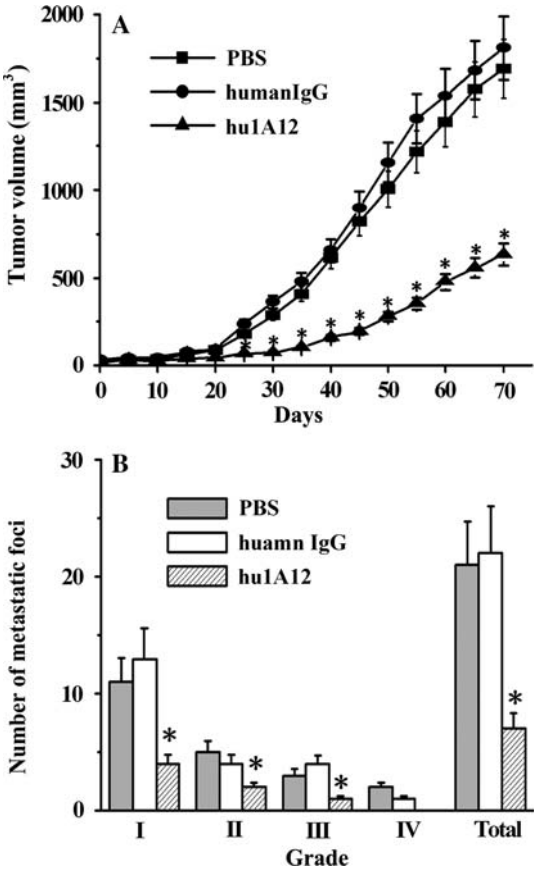

Fig. 6 hu1A12 effectively suppresses MDA-MB-435S tumor growth and spontaneous lung metastasis in nude mice. 5×10^6 MDA-MB-435S cells were orthotopically injected into the mfps of groups of 20 female nude mice. Then, the mice were treated with hu1A12 or control human IgG (5 mg/kg body weight, i.p.) twice per week for 4 weeks. For each group, ten animals were used to determine primary tumor growth rate and the other ten were used examine the extent of spontaneous lung metastases. **a** Efficacy of hu1A12 in inhibiting primary breast cancer growth. *Points* mean, *bars* SD; $*P < 0.05$ versus control human IgG. **b** The average number of lung metastatic foci for each group. *Columns* mean, *bars* SD; $*P < 0.05$ versus control human IgG (Mann–Whitney test)

Table 1 Metastasis incidence in PBS-, control IgG and hu1A12 treatment groups

Treatment	Lung	Lymph nodes	Other tissues
PBS	9/10	10/10	Brain 1/10
Control IgG	8/10	10/10	0/10
hu1A12	2/10	3/10	0/10

Table 2 Characterization of the epitope recognized by hu1A12

	Amino acid sequence	Frequency of clone
Selected sequences	DTENNNNGPSDX	(14/35)
	NAVNTNNAPTDY	(11/35)
	NALNHNNARSDY	(6/35)
	TTNPNNAPSSYA	(4/35)
Consensus motif	NAPSD	
Corresponding segment of human OPN	(210)DLNAPSDWD(218)	

Phage clones were isolated by panning the Ph.D.-12 Phage Display Peptide Library with hu1A12. Deduced amino acid sequences of inserts from selected phage clones were aligned for the consensus motif, which is indicated by underlined letters

indicated that OPN induces nuclear factor κB (NF-κB)-mediated promatrix metalloproteinase-2 activation through IκBα/IKK signaling pathways [44]. OPN enhances the cell motility and induces NF-κB-mediated uPA secretion through PI3-kinase/Akt/IKK-mediated signaling pathways [45]. As a survival factor, OPN regulates the activities of some of the Bcl-2 family of proteins. OPN maintains normal levels of anti-apoptotic molecules, Bcl-2 and Bcl-x_L, and decreases the amount of pro-apoptotic BAX in various other cell types [46, 47]. Therefore, the anti-apoptotic function of OPN might explain the metastatic potential of tumor cells that highly expressed OPN. The present study showed that hu1A12 could significantly inhibit OPN-mediated anti-apoptotic and prosurvival functions. Further data indicated that hu1A12 treatment could upregulate pro-apoptotic Bax expression and downregulate anti-apoptotic Bcl-2 expression in MDA-MB-435S cells. In OPN-treated MDA-MB-435S, the NF-κB pathway was activated, which provided a protective function to the cells. In contrast, cells pretreated with anti-OPN antibodies did not exhibit NF-κB activity. These results suggested that treatment with hu1A12 inhibited the anti-apoptotic function of OPN possibly through upregulating Bax, downregulating Bcl-2, and blocking the activation of NF-κB. In the in vivo study, hu1A12 showed significant efficacy in suppressing primary human breast tumor growth and spontaneous lung metastasis in nude mice, suggesting that it might have the potential to be a new therapeutic agent for the treatment of human breast cancer. To our knowledge, this is the first study reporting the in vivo antitumor effect of anti-OPN antibodies on breast cancer.

OPN contains several important functional domains including the integrin- and CD44-binding sites. OPN is thought to exert its pro-metastatic effects by mediating cell–matrix interactions and cellular signaling through binding with various integrins and CD44 receptors [2, 48]. For example, the ^{158}GRGDS^{162} sequence in human OPN contains a functional Arginine–Glycine–Asparate binding motif that ligates cell-surface αvβ3, αvβ1, αvβ5, and α5β1 integrins [2, 49, 50]. In this study, through screening of a phage display peptide library, the specific epitope recognized by the anti-OPN antibody 1A12 was identified to be

^{212}NAPSD^{216}, adjacent to the calcium-binding domain (amino acids 216–228) of OPN. Up to now, the function of the NAPSD motif has not yet been reported. In this study, we constructed five OPN single-point mutants: CM1 (212N to 212G), CM2 (213A to 213G), CM3 (214P to 214G), CM4 (215S to 215G) and CM5 (216D to 216G). Our data showed that all of the mutants had similar CD44- and $\alpha v\beta 3$ integrin-binding activity to wild type (data not shown), which suggested that the hu1A12 epitope NAPSD was not a critical domain for OPN binding to these receptors. Therefore, we speculate that hu1A12 inhibits OPN's function (OPN-induced cell migration, invasion, adhesion and colony formation) possibly by changing the conformation of OPN or by blocking the binding of OPN to OPN receptors via steric hindrance.

OPN is expressed by cells in a variety of tissues, including bone, dentin, cementum, hypertrophic cartilage, kidney, brain, vascular tissues and in distal renal tubules and in the gut, as well as in activated macrophages and lymphocytes. It is a multifunctional protein involved in various inflammatory processes, cell migration, and tissue remodeling. So blocking OPN signaling by treating with anti-OPN antibody may cause some extent of toxicity in humans, which may prevent anti-OPN antibody from being successful in the clinic. However, the previous study reported by Yamamoto et al. has demonstrated that cynomolgus monkeys well tolerated weakly injection of a chimeric anti-OPN antibody at a dose of 50 mg/kg four times. In their study, no obvious adverse effect and abnormal behavior of monkeys were observed [51]. Therefore, the anti-OPN antibody may have the potential to be well tolerated in humans. Currently, an evaluation of the preclinical toxicity of our humanized anti-OPN antibody in the cynomolgus monkey is under way.

In summary, the present data strongly support that OPN may be a target for the antibody-based therapies of breast cancer. Hu1A12, the humanized antibody specific for a new epitope of human OPN, has been demonstrated to be a potent antitumor agent in a mouse lung metastasis model of human breast cancer. Due to the expected low immunogenicity, hu1A12 is predicted to be more efficacious than the parental mouse antibody when used in humans.

Acknowledgments We thank Ms. Yang Yang and Ms. Jing Xu for their technical assistance as well as antibody production facility of National Engineering Research Center for Antibody Medicine for providing the purified control antibodies. This work was supported by National Natural Science Foundation of China, Ministry of Science & Technology of China (973 & 863 program projects), National Key Project for Infectious Disease, National Key New Drug Creation and Manufacturing Program and Shanghai Commission of Science & Technology. This study is also supported by Shanghai Leading Academic Discipline Project.

References

1. Denhardt DT, Guo X (1993) Osteopontin: a protein with diverse functions. FASEB J 7:1475–1482
2. Wai PY, Kuo PC (2004) The role of osteopontin in tumor metastasis. J Surg Res 21:228–241
3. Rodrigues LR, Teixeira JA, Schmitt FL, Paulsson M, Lindmark-Mänsson H (2007) The role of osteopontin in tumor progression and metastasis in breast cancer. Cancer Epidemiol Biomarkers Prev 16:1087–1097
4. Senger DR, Perruzzi CA, Papadopoulos A (1989) Elevated expression of secreted phosphoprotein I (osteopontin, 2ar) as a consequence of neoplastic transformation. Anticancer Res 9:1291–1299
5. Brown LF, Papadopoulos-Sergiou A, Berse B, Manseau EJ, Tognazzi K, Perruzzi CA, Dvorak HF, Senger DR (1994) Osteopontin expression and distribution in human carcinomas. Am J Pathol 145:610–623
6. Denhardt DT (1996) Oncogene-initiated aberrant signaling engenders the metastatic phenotype: synergistic transcription factor interactions are targets for cancer therapy. Crit Rev Oncogenes 7:261–291
7. Chakraborty G, Jain S, Patil TV, Kundu GC (2008) Down-regulation of osteopontin attenuates breast tumor progression in vivo. J Cell Mol Med. doi:10.1111/j.1582-4934.2008.00263.x
8. Behrend EI, Craig AM, Wilson SM, Denhardt DT, Chambers AF (1995) Expression of antisense osteopontin RNA in metastatic mouse fibroblasts is associated with reduced malignancy. Ann N Y Acad Sci 760:299–301
9. Behrend EI, Craig AM, Wilson SM, Denhardt DT, Chambers AF (1994) Reduced malignancy of ras-transformed NIH 3T3 cells expressing antisense osteopontin RNA. Cancer Res 54:832–837
10. Adwan H, Bäuerle T, Najajreh Y, Elazer V, Golomb G, Berger MR (2004) Decreased levels of osteopontin and bone sialoprotein II are correlated with reduced proliferation, colony formation, and migration of GFP-MDA-MB-231 cells. Int J Oncol 24:1235–1244
11. Wai PY, Mi Z, Guo H, Sarraf-Yazdi S, Gao C, Wei J, Marroquin CE, Clary B, Kuo PC (2005) Osteopontin silencing by small interfering RNA suppresses in vitro and in vivo CT26 murine colon adenocarcinoma metastasis. Carcinogenesis 26:741–751
12. Cui R, Takahashi F, Ohashi R, Gu T, Yoshioka M, Nishio K, Ohe Y, Tominaga S, Takagi Y, Sasaki S, Fukuchi Y, Takahashi K (2007) Abrogation of the interaction between osteopontin and alphavbeta3 integrin reduces tumor growth of human lung cancer cells in mice. Lung Cancer 57:302–310
13. Allan AL, George R, Vantyghem SA (2006) Role of the integrin-binding protein osteopontin in lymphatic metastasis of breast cancer. Am J Pathol 169:233–246
14. Chambers AF, Groom AC, MacDonald IC (2002) Dissemination and growth of cancer cells in metastatic sites. Nat Rev Cancer 2:563–572
15. Cole BF, Gelber RD, Gelber S, Coates AS, Goldhirsch A (2001) Polychemotherapy for early breast cancer: an overview of the randomised clinical trials with quality-adjusted survival analysis. Lancet 358:277–286
16. Clarke M, Collins R, Darby S, Davies C, Elphinstone P, Evans E, Godwin J, Gray R, Hicks C, James S, MacKinnon E, McGale P, McHugh T, Peto R, Taylor C, Wang Y, Early Breast Cancer Trialists' Collaborative Group (EBCTCG) (2005) Effects of radiotherapy and of differences in the extent of surgery for early breast cancer on local recurrence and 15-year survival: an overview of the randomised trials. Lancet 366:2087–2106
17. Singhal H, Bautista DS, Tonkin KS, O'Malley FP, Tuck AB, Chambers AF, Harris JF (1997) Elevated plasma osteopontin in

metastatic breast cancer associated with increased tumor burden and decreased survival. Clin Cancer Res 3:605–611
18. Tuck AB, O'Malley FP, Singhal H, Harris JF, Tonkin KS, Kerkvliet N, Saad Z, Doig GS, Chambers AF (1998) Osteopontin expression in a group of lymph node negative breast cancer patients. Int J Cancer 79:502–508
19. Coppola D, Szabo M, Boulware D, Muraca P, Alsarraj M, Chambers AF, Yeatman TJ (2004) Correlation of osteopontin protein expression and pathological stage across a wide variety of tumor histologies. Clin Cancer Res 10:184–190
20. Rudland PS, Platt-Higgins A, El-Tanani M, De Silva Rudland S, Barraclough R, Winstanley JH, Howitt R, West CR (2002) Prognostic significance of the metastasis-associated protein osteopontin in human breast cancer. Cancer Res 62:3417–3427
21. Tuck AB, Arsenault DM, O'Malley FP, Hota C, Ling MC, Wilson SM, Chambers AF (1999) Osteopontin induces increased invasiveness and plasminogen activator expression of human mammary epithelial cells. Oncogene 18:4237–4246
22. Shevde LA, Samant RS, Paik JC, Metge BJ, Chambers AF, Casey G, Frost AR, Welch DR (2006) Osteopontin knockdown suppresses tumorigenicity of human metastatic breast carcinoma, MDA-MB-435. Clin Exp Metastasis 23:123–133
23. Suzuki M, Mose E, Galloy C, Tarin D (2007) Osteopontin gene expression determines spontaneous metastatic performance of orthotopic human breast cancer xenografts. Am J Pathol 171:682–692
24. Bautista DS, Xuan JW, Hota C, Chambers AF, Harris JF (1994) Inhibition of Arg-Gly-Asp (RGD)-mediated cell adhesion to osteopontin by a monoclonal antibody against osteopontin. J Biol Chem 269:23280–23285
25. Li B, Wang H, Dai J, Ji J, Qian W, Zhang D, Hou S, Guo Y (2005) Construction and characterization of a humanized anti-human CD3 monoclonal antibody 12F6 with effective immunoregulation functions. Immunology 116:487–498
26. Queen C, Schneider WP, Selick HE, Payne PW, Landolfi NF, Duncan JF, Avdalovic NM, Levitt M, Junghans RP, Waldmann TA (1989) A humanized antibody that binds to the interleukin 2 receptor. Proc Natl Acad Sci USA 86:10029–10033
27. Pulito VL, Roberts VA, Adair JR, Rothermel AL, Collins AM, Varga SS, Martocello C, Bodmer M, Jolliffe LK, Zivin RA (1996) Humanization and molecular modeling of the anti-CD4 monoclonal antibody, OKT4A. J Immunol 156:2840–2850
28. Kettleborough CA, Saldanha J, Heath VJ, Morrison CJ, Bendig MM (1991) Humanization of a mouse monoclonal antibody by CDR-grafting: the importance of framework residues on loop conformation. Protein Eng 4:773–783
29. Ye QH, Qin LX, Forgues M, He P, Kim JW, Peng AC, Simon R, Li Y, Robles AI, Chen Y, Ma ZC, Wu ZQ, Ye SL, Liu YK, Tang ZY, Wang XW (2003) Predicting hepatitis B virus-positive metastatic hepatocellular carcinomas using gene expression profiling and supervised machine learning. Nat Med 9:416–423
30. Fan K, Dai J, Wang H, Wei H, Cao Z, Hou S, Qian W, Wang H, Li B, Zhao J, Xu H, Yang C, Guo Y (2008) Treatment of collagen-induced arthritis with an anti-osteopontin monoclonal antibody through promotion of apoptosis of both murine and human activated T cells. Arthritis Rheum 58:2041–2052
31. Kabat EA, Wu TT, Reid-Miller M, Perry HM, Gottesman KS (1987) Sequences of proteins of immunological interest, 4th edn. United States Department of Health and Human Services, Washington, DC
32. Schroff RW, Foon KA, Beatty SM, Oldham RK, Morgan AC Jr (1985) Human anti-murine immunoglobulin responses in patients receiving monoclonal antibody therapy. Cancer Res 45:879–885
33. Owens RJ, Young RJ (1994) The genetic engineering of monoclonal antibodies. J Immunol Methods 168:149–165
34. Morrison SL, Johnson MJ, Herzenberg LA, Oi VT (1984) Chimeric human antibody molecules: mouse antigen-binding domains with human constant region domains. Proc Natl Acad Sci USA 81:6851–6855
35. Boulianne GL, Hozumi N, Shulman MJ (1984) Production of functional chimaeric mouse/human antibody. Nature 312:643–646
36. Jones PT, Dear PH, Foote J, Neuberger MS, Winter G (1986) Replacing the complementarity-determining regions in a human antibody with those from a mouse. Nature 321:522–525
37. Winter G, Harris WJ (1993) Humanized antibodies. Immunol Today 14:243–246
38. Kipriyanov SM, Le Gall F (2004) Generation and production of engineered antibodies. Mol Biotechnol 26:39–60
39. Presta LG, Lahr SJ, Shields RL (1993) Humanization of an antibody directed against IgE. J Immunol 151:2623–2632
40. Furger KA, Menon RK, Tuck AB, Bramwell VH, Chambers AF (2001) The functional and clinical roles of osteopontin in cancer and metastasis. Curr Mol Med 1:621–632
41. Xuan JW, Hota C, Chambers AF (1994) Recombinant GST-human osteopontin fusion protein is functional in RGD-dependent cell adhesion. J Cell Biochem 54:247–255
42. Senger DR, Perruzzi CA (1996) Cell migration promoted by a potent GRGDS-containing thrombin-cleavage fragment of osteopontin. Biochim Biophys Acta 1314:13–24
43. Tuck AB, Chambers AF (2001) The role of osteopontin in breast cancer: clinical and experimental studies. J Mammary Gland Biol Neoplasia 6:419–429
44. Philip S, Kundu GC (2003) Osteopontin induces nuclear factor κB-mediated promatrix metalloproteinase-2 activation through IκBα/IKK signaling pathways, and curcumin (diferulolylmethane) down-regulates these pathways. J Biol Chem 278:14487–14497
45. Das R, Mahabeleshwar GH, Kundu GC (2003) Osteopontin stimulates cell motility and nuclear factor B-mediated secretion of urokinase type plasminogen activator through phosphatidylinositol 3-kinase/Akt signaling pathways in breast cancer cells. J Biol Chem 278:28593–28606
46. Xu H, Jin XQ, Jing L, Li GS (2006) Effect of sodium fluoride on the expression of Bcl-2 family and osteopontin in rat renal tubular cells. Biol Trace Elem Res 109:55–60
47. Hashimoto M, Sun D, Rittling SR, Denhardt DT, Young W (2007) Osteopontin-deficient mice exhibit less inflammation, greater tissue damage, and impaired locomotor recovery from spinal cord injury compared with wild-type controls. J Neurosci 27:3603–3611
48. Rangaswami H, Bulbule A, Kundu GC (2006) Osteopontin: role in cell signaling and cancer progression. Trends Cell Biol 16:79–87
49. Hijiya N, Setoguchi M, Matsuura K, Higuchi Y, Akizuki S, Yamamoto S (1994) Cloning and characterization of the human osteopontin gene and its promoter. Biochem J 303:255–262
50. O'Regan A, Berman JS (2000) Osteopontin: a key cytokine in cell-mediated and granulomatous inflammation. Int J Exp Pathol 81:373–390
51. Yamamoto N, Nakashima T, Torikai M, Naruse T, Morimoto J, Kon S, Sakai F, Uede T (2007) Successful treatment of collagen-induced arthritis in non-human primates by chimeric anti-osteopontin antibody. Int Immunopharmacol 7:1460–1470